Research article Available online www.ijsrr.org ISSN: 2279–0543

International Journal of Scientific Research and Reviews

Nucleation and Growth of Bismuth Telluride Dendritic Nanostructures Via Electrodeposition Method

Khairnar V.S. [1]*, Kulkarni A. N. [2], Lonikar V. V. [2], Gite A. B. [3], Waghmare R.V.[1]

[1]Department of Physics, Vidya Bharati Mahavidalaya, Amravati- 444602, India.
[2]Department of Physics, School of Science, Sandip University, Nashik 422002, India.
[3]Department of Physics, SNJB's Arts and Science College, Nashik 422101, India.

ABSTRACT

Bismuth Telluride (Bi_2Te_3) dendritic nanostructures were prepared on stainless steel substrate by electrochemical deposition from an aqueous solution of bismuth nitrate and tellurium dioxide in the presence of nitric acid. The structural and morphological properties of the deposited films were investigated as a function of applied deposition voltage. X-ray diffractometric studies confirmed the rhombohedral phase of Bi_2Te_3 crystals in the deposited films. The deposition potential apparently was found to be playing a significant role in controlling the reaction rate resulting in the evolution of dendritic Bi_2Te_3 crystals with preferred orientation along (0 0 15) hkl plane. These Bi_2Te_3 nanocrystals can be used effectively in variety of applications such as thermoelectric refrigeration, thermoelectric generator (TEG), thermoelectric cooling (TEC), thermal sensor etc.

KEYWORDS: Electrode position; Bismuth Telluride (Bi_2Te_3); applied deposition potential; dendritic nanostructure; orientated attachment growth

***Corresponding author**

V.S. Khairnar

Research Scholar, Department of Physics,

Vidya Bharati Mahavidalaya,

Amravati- 444602, India.

Email: khairnar.vinod@gmail.com, Contact no. +919326666608

INTRODUCTION

Of-late, synthesis of semiconductor chalcogenides with different noble nanostructures have been attracting great attention over past few years because of their peerless electrical, morphological and thermal properties [1-3]. These inherent properties the metal chalcogenides offer due to their shape, morphology and crystallinity, which make them potential candidates suitable for many applications such as energy harvesting thermoelectric and storage devices [4-10] and sensors [11]. Thus, in recent years, there has been a large interest in the research of synthesis of noble nanostructures with defined shapes and preferred crystallinity [12-15]**.** Out of the numerous morphological nanostructures, the dendritic nanostructures open up new possibilities for their applications [16-18]. This may be due to their large surface area composed of trunks and branches, resulting in good electrical and thermal conductivity [19].

Recently various experimental studies have been carried out to obtain Bi_2Te_3 dendritic nanostructures through different methods [8, 20-24]. However, many reports on the synthesis of Bi_2Te_3 reveal that, the morphologies obtained are rough and porous, which results in a lower power factor [25]. Therefore, the synthesis of symmetrical and well defined dendritic shaped Bi_2Te_3 nanostructures is still a challenging field of research.

Among all these techniques, electrodeposition is one of the simplest and facile ways for the controlled synthesis of dendritic structures. This is because; the applied potential plays the role of a driving force, which guides the ions in the electrolyte. This in turn decides the growth rate of nanostructures on the substrates during the electrodeposition [26].

In the present work, Bi_2Te_3 dendritic nanostructures consisting of lily flowers having preferred orientation along (0 0 15) were synthesized via a simple electrodeposition technique. The growth mechanism of the dendritic nanostructure was analyzed on the basis of the orientated attachment model.

EXPERIMENTAL DETAILS

Electrodeposition of Bi_2Te_3 films

In the present synthesis, solutions of bismuth nitrate ($Bi_2(NO_3)_3.5H_2O$) and tellurium dioxide (TeO_2) were prepared in nitric acid (HNO_3), respectively in two different beakers, wherein $Bi_2(NO_3)_3.5H_2O$ acts as a precursor of Bi^{3+} and TeO_2, that of Te^{2-}explained in the following steps.

First, the bath of 7.5 mM Bi^{3+} was prepared by adding 0.90 gm of bismuth nitrate in 250 ml of 1M nitric acid and kept for 15 min until a uniform mixture was formed. Second, 0.1 M Ethylene Diamine tetra acetic acid (EDTA), a complexing agent was then prepared in 100 ml double distilled

water. Third, 3ml of 0.1M EDTA then added to the first bath containing bismuth source to obtain Bi^{3+}- EDTA complex. Fourth, 10 mM solution was prepared in 1M (250 ml) of nitric acid under constant stirring at 80℃ temperature for 30 min. Fifth, 13.5 ml of Te^{2-} precursor solution was slowly introduced into the 16.5ml that of Bi^{3+}-EDTA complex precursor solution under constant stirring. The reaction is considered to be based on slow release of Bi^{3+} and Te^{2-} ions in the presence of EDTA, which, helps for obtaining the soluble species of the Bi^{3+} in acidic medium during the synthesis process [27]**.** The electrodeposition was carried out for various applied potentials viz. -350, -400, -450, -500, -550 and -600 mV w.r.t. Standard Calomel Electrode (SCE) at room temperature for the deposition time of 40 min and named as a-f respectively.

Structural analysis and phase detection of the Bi_2Te_3 crystals in the electrodeposited films were carried out with the help of Panalytical Xpert PRO X-Ray Diffractometer with Cu Kα radiation (λ = 1.5405 A˚). Surface morphology and compositional analysis were carried out using a scanning electron microscope (SEM) and an energy dispersive X-ray analysis setup (EDXS) attached with SEM (model: JEOL-JSM 6360) and respectively.

RESULTS AND DISCUSSIONS

X-ray diffraction studies of Bi_2Te_3 thin films

Fig.1 shows XRD patterns for samples a–f. It can be seen from fig. 1 (A) that diffractograms for samples a-d have a defined peaks around 2θ ~ 27.66˚, 38.83˚, 41.14˚, 44.57˚, and 50.31˚ corresponding to the hkl planes (0 1 5), (1 0 10), (1 1 0), (0 0 15) and (2 0 5), respectively. The observed peaks were compared with standard diffraction values of JCPDS card No: 15-0863, which confirms the rhombohedral phase of Bi_2Te_3 crystals in the deposited films. However, fig. 2 (B) shows that samples a-d have the polycrystalline nature with maximum intensity signature peak along (0 1 5) around 2θ ~ 27.66˚. Interestingly, at deposition potential of -550 mV the sample “e” showed preferred orientation along (0 0 15) around 2θ ~ 44.57˚. The dominant peak along (0 1 5) around 2θ ~ 27.66˚ observed, gets broader as you go from the sample “a to e”. However, in case of sample ‘f’, the obtained XRD pattern has the signatures same as samples a-d.

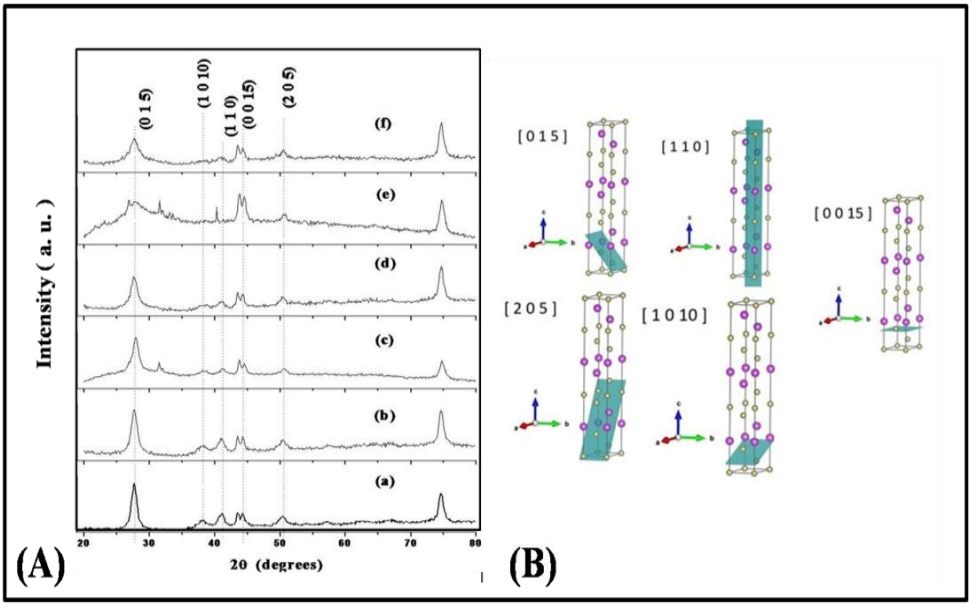

Fig1. (A) X-ray diffraction patterns of sample (a-f) (B) Crystallographic plans observed for samples (a-f).

Such obtained X-ray diffraction patterns can be discussed on the basis of the regular growth and kinetics of crystals in electrodeposition technique, presented in fig. 2 (A-C). Generally, in case of electrochemical deposition the nucleation and growth is guided by the various parameters viz. temperature, pH, concentration and potential gradient created by the electrodes.

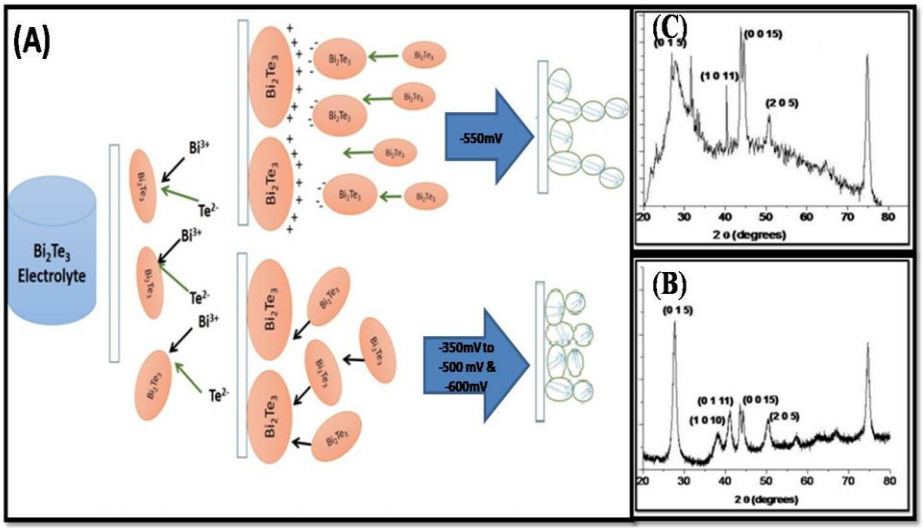

Fig2. (A) Schematic showing probable mechanism of formation of observed crystalline phases for samples (a-f), (B) X-ray diffractograms for samples (a-d), (C) X-ray diffractograms for of sample (e).

It appears that in samples a-d, the nucleation and growth of nanocrystals are purely driven by the thermodynamic potential[28]. The mechanism of crystal growth in electrodeposition is a well understood phenomenon [29-30]. Generally, in deposition, the ions or molecules in the reaction bath collide with each other and form embryos. These embryos are a result of precipitation and coagulation of ions in the solution for which the equilibrium state is decided by the thermodynamic potentials. The embryos have a critical size below which they re-dissolve into the solution and are

thus, thermodynamically unstable. However, in heterogeneous nucleation like the present case, the deposition potential along with thermodynamic potential may have electrically guided the embryos towards the substrate during the deposition. This lowers the energy required for the formation of interface between the embryo and the solid substrate, which, initiate the nucleation over the surface of electrode. Further, the cationic and anionic species in the solution to be deposited get electrically guided and deposited over the embryo and start growing into a crystal. In general, during deposition where thermal treatment is not involved, the crystals start growing along the geometric orientations as a function of deposition potential, which minimize the energy configuration of the system [31]. This is presented using schematic in fig. 2 (A) and XRD for samples a-d in fig. 2 (B).

Thus, as discussed above, in case of sample "e", the process of nucleation and growth dynamics is observed to be driven by both the electrical potential and thermodynamic potential. This may be a because of the redistribution of charge densities in the crystal lattice at particular potential of -550 mV. This results in the growth of Bi_2Te_3 crystals having a preferred orientation along (0 0 15) as shown in schematic fig. 2 (A) and XRD for sample 'e' in fig. 2 (C).

At the same time, in case of sample 'e', as discussed above, the nucleation and growth may have been driven by the combination of the deposition potential and thermodynamic potential. This might have resulted in crystal strain due to which the broadening of the peak (0 1 5) around $2\theta \sim 27.66^{\circ}$is observed in XRD for sample 'e' in fig. 2 (C).

Further, in case of sample 'f' the nucleation and growth may have been dominated by the deposition potential over thermodynamic potential. This might have resulted development of defects due to the rapid but haphazard growth unlike sample 'e', forced by the electro-deposition potential. Thus, in case of sample 'f' XRD pattern indicates the presence of individual unit cells and no preferred direction of growth, which is in agreement with the morphology for sample 'f'. Further the (0 1 5) peak is sharp again which indicates absence of strain in the unit cell since there is no competition between the two growth mechanisms.

In addition, the induced micro-strain and dislocation density measurement have been carried out along (015) plane for samples a-f and tabulated in Table 1. However, the variation of obtained values of strains versus deposition potential are plotted and presented in fig. 3 (A, B), which in agreement with the above discussion.

The correction for the instrumental broadening was carried out by using the corundum standard sample. Further, diffraction peak broadening due the induced micro strain has also been removed by using standard method from literature [32].

Table 1: Induced micro strain and dislocation density measurements along (015) plane for samples (a-f):

Deposition Potentials	2θ (degrees)	d- spacing in A°	FWHM β [°2Th.]	Crystallite Size , D (nm)	Micro strain ε (10^{-4} lin^{-2} m^{-4})	Dislocation Density δ (10^{16} line/m^2)
-350 Mv	27.7	3.220	0.962	8.88	**40.75**	**157.18**
-400 mV	27.68	3.223	1.139	7.50	**48.26**	**220.35**
-450 mV	27.92	3.195	1.099	7.78	**46.54**	**204.94**
-500 mV	27.68	3.223	1.194	7.15	**50.59**	**242.15**
-550 mV	27.72	3.218	1.342	2.69	**134.59**	**1714**
-600 mV	27.69	3.221	1.497	5.71	**63.42**	**380.63**

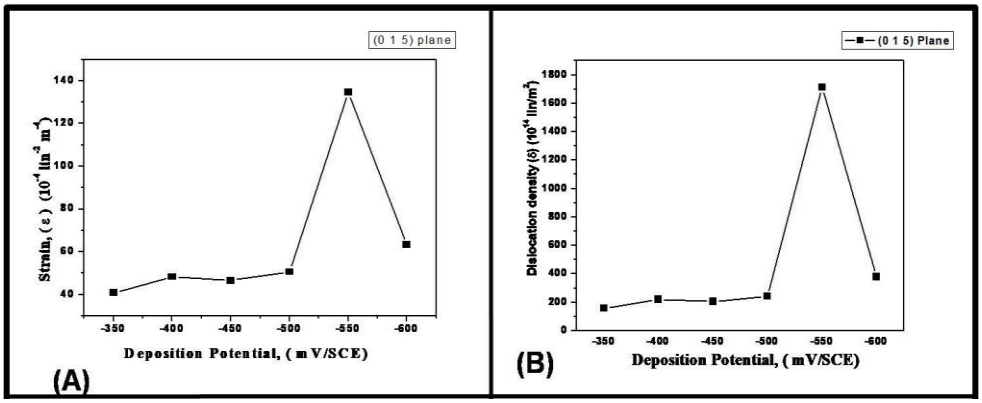

Fig3. Variation of (A) induced micro strain (B) dislocation density as a function of deposition potential along (015) plane for samples (a-f).

Morphological studies of Bi_2Te_3 thin films:

Fig.4 represents the typical beautiful SEM images of as prepared Bi_2Te_3 dendritic nanostructures for different deposition potentials. At the initial stage of electrodeposition some dendritic nuclei of bismuth telluride were found on the rough surface of the substrate along with a few smaller dendritic nanostructures (Sample a). Further, the electric field around the substrate led to the deposition of Bi_2Te_3 crystals on the surface of already existing particles and nanoparticles start reforming initially into spheres (Sample b) and then in agglomeration of the spheres (Sample c & d). Further diffusion of Bi_2Te_3 ions may lead to the nucleation of Bi_2Te_3 crystals on the trunk that finally resulted in the formation of dendrite structures (sample e). The diameter of the branches is observed about 37–100 nm.

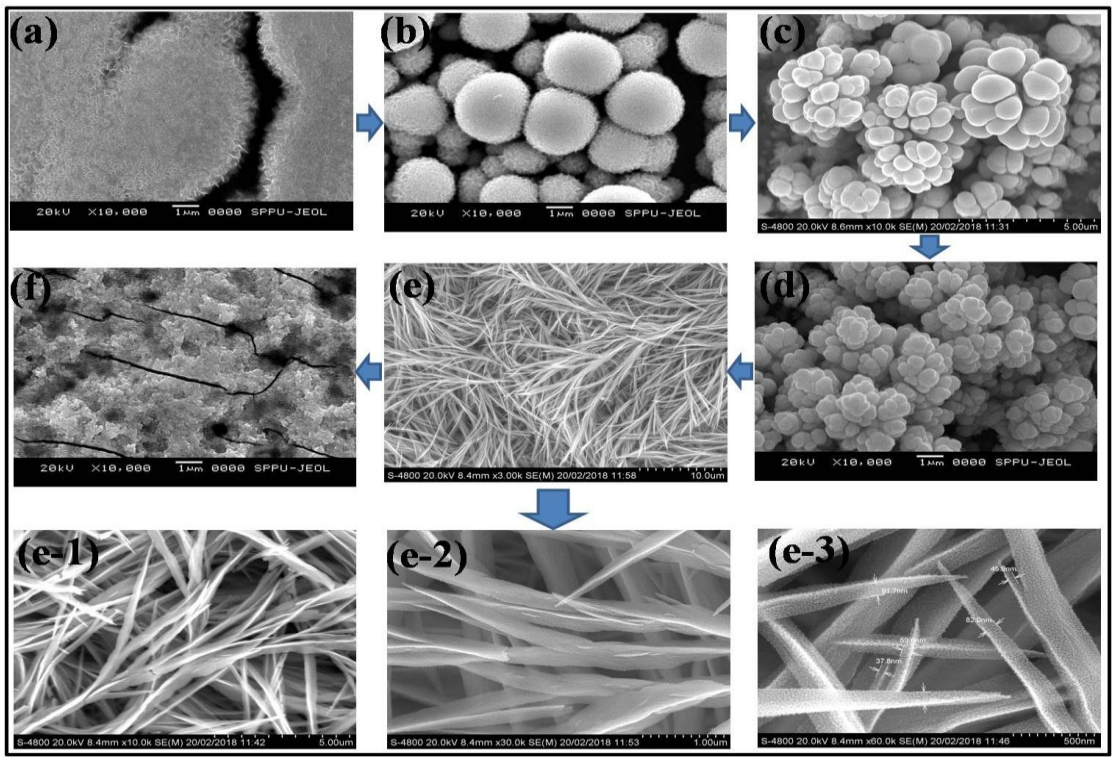

Fig4. Scanning Electron Micrographs of samples (a-f).

Growth analysis of Bi_2Te_3 crystals in electrodeposited thin films

The evolution of different morphologies a function of deposition potential are explained on the basis of thermodynamic nucleation and growth along with oriented attachment mechanism and presented with the help of growth schematic as shown in fig. 5(a-e).

Initially, SEM image of sample "a" presented in fig. 4(a) show uniformly distributed Bi_2Te_3 dendrites. Further, as seen from SEM image shown in fig. 4(b), sample "b" electrodeposited at -400 mV, showed agglomerated morphology. These indicate that, during electrodeposition at room temperature, the thermodynamic potentials may have dominated the deposition potential and initiated the nucleation and growth. And thus, schematic shown in fig. 5 (b), reveals how crystals in sample "b" acquire spongy spherical morphology in order to minimize the surface energy [33].

These agglomerates seem to be guided towards each other to have the morphology as seen in the SEM image presented in fig. 4(c-d). It may be argued that, as we increase the potential, electrodeposition potential along with the thermodynamic potential both, drive the nucleation and growth processes. This may have leaded the growth by oriented attachment of the spherical agglomerates, as shown by the growth schematic in fig. 5(c-d).

Further, as we see that, in case of sample "e", with enhanced deposition potential, the nucleation and growth observed to be completely dominated by the deposition potential over thermodynamic potential. This is evident from the lily flower-like dendrites formed by small spongy

spheres. This is because, at higher deposition potential such as -550mV, the stronger electric force on the embryos formed in the electrolyte is causing the coagulation before they could grow bigger and become unstable due to thermodynamic potentials. Thus, during the initial stage, embryos get guided by the electrodeposition potential and grow as spongy spheres of smaller size as shown in fig. 4(e-3).

Since, during the study, deposition potential is the only parameter that is been varied, it may be argued that, the smaller size of agglomerates and their growth by attachment to each other is observed to be accelerated with the electrodeposition potential from sample a-e. Thus, the time available for the Bi^{3+} and Te^{2-} to nucleate and grow is limited and thus, allowed the agglomerates to grow to smaller sizes. At the same time, it may have favored the oriented attachment of the small spongy spheres to have lily flower like morphology as shown in schematic in fig. 5(e). Such oriented attachment growth in particular direction of the crystal is evident from the change in the intensity of the X-ray diffraction peaks along (0 0 15) plane.

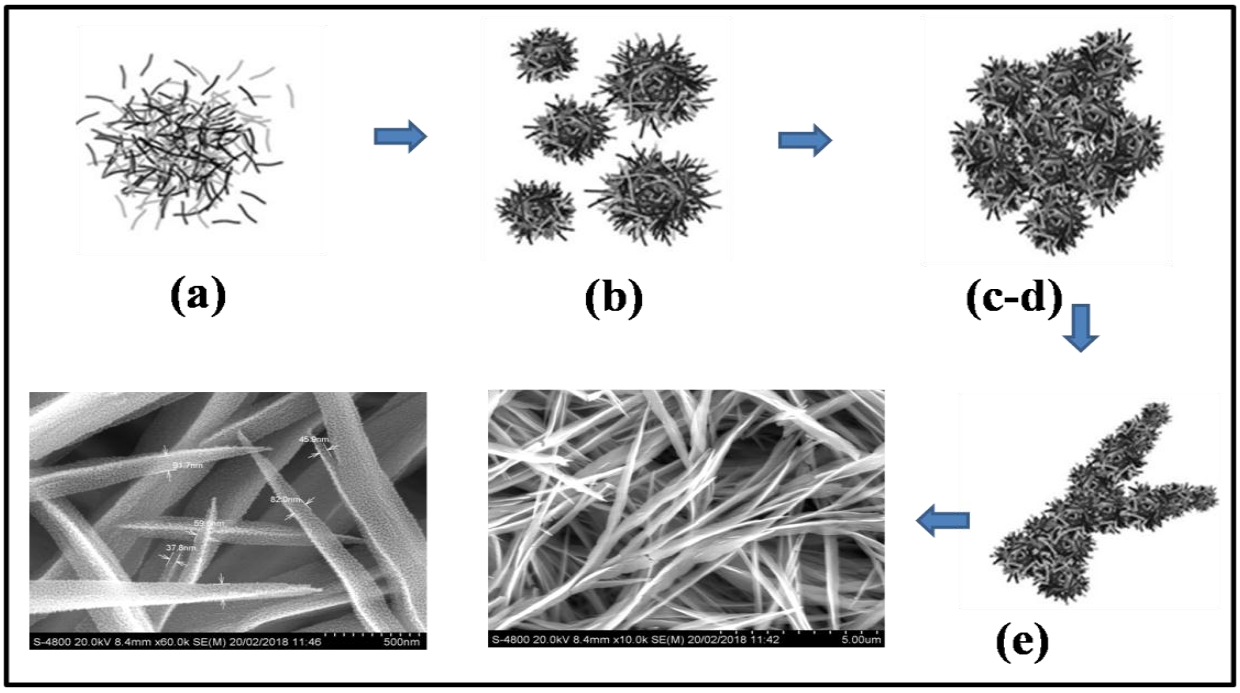

Fig5. Schematic showing probable growth mechanism of samples (a-e).

In case of sample 'f' the growth is fully controlled by the deposition potential and the growth seems to be haphazard since there may be more than one places of low electric potential for the nuclei to attach on the deposited mass. The deposition potential of -600mV does not allow the nuclei to get oriented in a particular direction as shown in fig. 4(f).

Elemental studies of Bi_2Te_3 thin films

The elemental analysis of the electrodeposited Bi_2Te_3 film samples (a-f) was carried out using an energy dispersive X-ray spectroscopy (EDXS). Fig. 6 shows that average atomic percentages of

Bi and Te are found to be controlled by the deposition potential. Besides that, the Bi-rich telluride compounds are formed from sample a-f. This may be because of enhanced reduction reaction of Bi^{3+}, which is controlled by deposition potential along with TeO_2^{2+} reduction to form Bi_2Te_3 compounds on stainless steel substrates with slightly different stoichiometry [34].

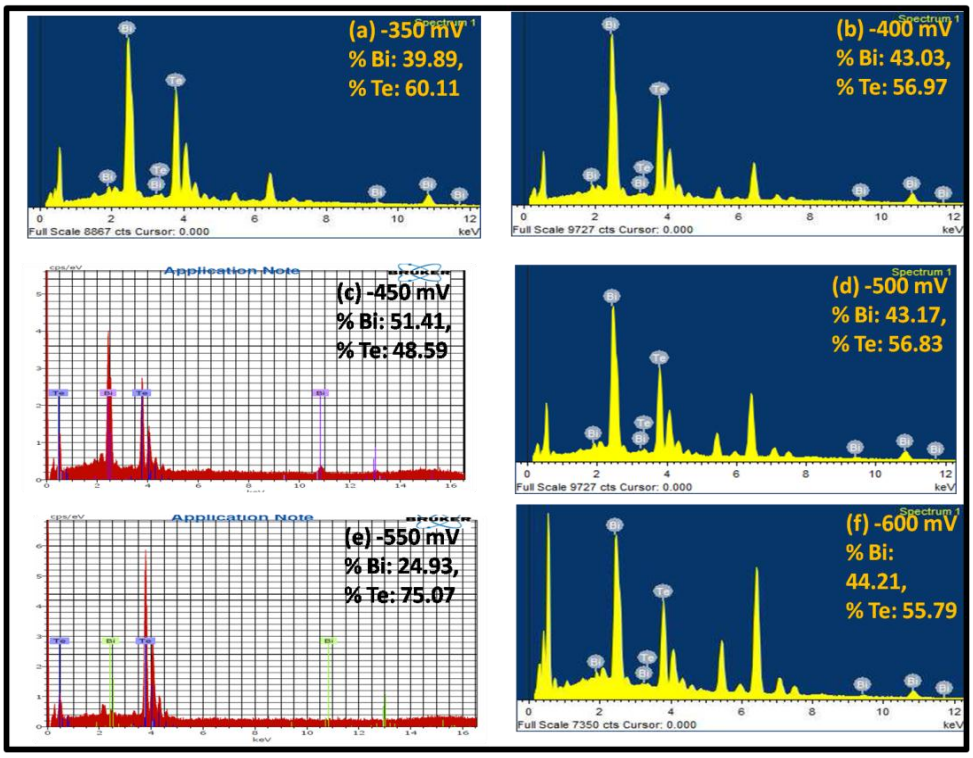

Fig 6. Typical EDXS spectra for samples (a-f).

CONCLUSIONS

To summarize, the Bi_2Te_3 dendritic nanostructures have been synthesized on stainless steel substrate by ELECTRODEPOSITION. The advantage of this technique reported here is that, the morphology of dendritic nanostructure can be varied with deposition potential. Series of scanning electron micrograph images revealed evolution of beautiful oriented dendritic structures as a function of deposition potential. This is in agreement with the discussion of preferred growth of crystals in deposited Bi_2Te_3 films. The growth mechanism of synthesized dendritic nanostructures was explained by the oriented attachment mechanism. This nanostructure may have important applications in thermoelectric refrigeration, thermoelectric generator (TEG), thermoelectric cooling (TEC), thermal sensor etc.

ACKNOWLEDGMENTS

VSK is thankful to Department of Physics, Vidya Bharati Mahavidalaya, Amravati, for lab support, Department of Engineering Physics, MET's Institute of Engineering, Nasik for support and encouragement, also thankful to Department of Physics, Sandip University, Nashik for extending

their cooperation and encouragement. VSK is grateful to Dr. V. P. Wani, Principal MET's Institute of Engineering, Nashik and Dr. R. S. Patil, Principal PSGVP College Shahada. ANK and VVL grateful to management of Sandip University, Nashik for support and encouragement.

REFERENCES

1. Hicks LD, Dresselhaus MS. Effect of quantum- well structures on the thermoelectric figure of merit. Phys. Rev. B, 1993; (47): 12727–12731..
2. Hicks LD, Harman TC, Sun X, Dresselhaus MS. Experimental study of the effect of quantum-well structures on the thermoelectric figure of merit. Phys. Rev. B., 1996; (53): R10493–R10496.
3. Hicks LD, Dresselhaus MS. Thermoelectric figure of merit of a one-dimensional conductor. Phys. Rev. B 1993; (43): 16631–16634.
4. Ota T, Uesugi T, Tokiai T, Nosaka M. $(Bi,Sb)_2$ $(Te,Se)_3$ type n- type thermoelectric element by a single element pulverized mixed solid phase reaction method. Trans. Inst. Electr. Eng. Japan. 1991; 111–B 670.
5. Hava S, Sequeira H, Hunsperger R. Thermoelectric and thermal properties of GaAlAs Peltier cooled laser diodes, Journal of applied physics. 1985; 58(5): 1727-1732.
6. Akshay VR, Suneesh MV, and Vasundhara M. Tailoring Thermoelectric Properties through Structure and Morphology in Chemically Synthesized n-Type Bismuth Telluride Nanostructures. Inorg. Chem., 2017; 56(11): 6264–6274.
7. Kiely J, Dong HL. Characteristics of Bi0.5Sb1.5Te3/Be2Te2.4Se0.6 thin-film thermoelectric devices for power generation. Meas. Sci. Technol, 1997; (8): 661–665.
8. Zhang C, Fan XA. Fan, Hu J, Jiang CU, Xiang Q, Guangqiang Li, Yawei Li, Zhu He. Changing the Band Gaps by Controlling the Distribution of Initial Particle Size to Improve the Power Factor of N-Type Bi2Te3 Based Polycrystalline Bulks. Advance Engineering Materials, 2017; (19): 1–8.
9. Lou DY. Characterization of optical disks, Appl. Opt. 1982; (21): 1602.
10. CaoZ, Koukharenko E, Tudor MJ, Torah R, Beeby SP. Flexible screen printed thermoelectric generator with enhanced processes and materials. Sensors Actuators, A Phys. 2016; (238).
11. Kim MY, & Oh TS. Thermoelectric characteristics of the thermopile sensors processed with the electrodeposited Bi–Te and Sb–Te thin films. Surface review and letters, 2010; 17(03): 311–316
12. Thorat JB, Mohite SV, Bagade AA, Shinde TJ, Fulari VJ, Rajpure KY, Shinde NS. Nanocrystalline Bi2Te3thin films synthesized by electrodeposition method for

photoelectrochemical application. Mater. Sci. Semicond. Process, 2018; (79): 119–126.

13. Qu W, Plötner M, Fische WJ. Microfabrication of thermoelectric generators on flexible foil substrates as a power source for autonomous microsystems, J. Micromechanics Microengineering, 2001; (11): 146–152.
14. Song Y, Yoo IJ, Heo NR, Lim DC, Lee D, Lee JY, Lee KH, Kim KH, Lim JH. Electrodeposition of thermoelectric Bi2Te3thin films with added surfactant. Curr. Appl. Phys, 2015; (15): 261–264.
15. Kang WS, Li WJ, Chou WC, Tseng MF, Lin SC. Microstructure and thermoelectric properties of Bi2Te3electrodeposits plated in nitric and hydrochloric acid baths. Thin Solid Films,2017; (623): 90–97.
16. Patil PB, Mali SS, Kondalkar VV, Mane RR, Patil PS, Hong CK, Bhosale PN. Morphologically controlled electrodeposition of fern shaped Bi2Te3 thin films for photoelectrochemical performance. J. Electroanal. Chem. 2015; (758): 178–190.
17. Dong T, Yuan RH, Shi YG, Wang NL. Temperature-Induced Plasma Frequency Shift in Bi2Te3 and CuxBi2Se3. Chinese Physics Letter 2013; 13(12): 127801
18. Erickson KJ, Limmer SJ, Yelton WG, Rochford C, Siegal MP, and Medlin DL. Evolution of Microstructural Disorder in Annealed Bismuth Telluride Nanowires. ECS J. Solid State Sci. Technol., 2017; 6(3): N3117–N3124.
19. Cao Y, Zeng Z, Liu Y, Zhang X, Shen C, Wang X, Gan Z, Wu H, Hu Z. Electrodeposition and Thermoelectric Characterization of (00L)-Oriented Bi2Te3 Thin Films on Silicon with Seed Layer. J. Electrochem. Soc, 2013; (160): D565–D569
20. Antonenko AO, Charnaya EV, Nefedov DY, Podorozhkin DY, Uskov AV, Bugaev AS, Lee MK, Chang LG, Naumov SV, Perevozchikova YA, Chistyakov VV, Huang JCA, Marchenkov VV. NMR studies of the topological insulator Bi2Te3. 2017; (59): 1–15.
21. Luo B, Deng Y, Wang Y, Gao M, Zhu W, Hashim HT, García-Cañadas JC. Synergistic photovoltaic–thermoelectric effect in a nanostructured CdTe/Bi_2Te_3 heterojunction for hybrid energy harvesting. RSC Adv, 2016; (6): 114046–114051.
22. Wu K, Yan Y, Zhang J, Mao Y, Xie H, Yang J, Zhang Q, Uher C, Tang X. Preparation of n-type Bi_2 Te_3 thermoelectric materials by non-contact dispenser printing combined with selective laser melting. Phys. Status Solid - Rapid Res. Lett., 2017; (11): 1700067.
23. Gaul A, Peng Q, Singh DJ, Ramanath G, Borca-Tasciuc T. Pressure-induced insulator-to-metal transitions for enhancing thermoelectric power factor in bismuth telluride-based alloys. Phys. Chem. Chem. Phys., 2017; (19): 12784–12793.
24. Mahmud KH, Yudistirani SA, Ramadhan AI. Analysis Of Power Characteristics Of Model

Thermoelectric Generator (TEG) Small Modular. Int. J. Sci. Technol. Res, 2017; (60).

25. Lee J, Kim Y, Cagnon L, Gösele U, Lee J, Nielsch K. Power factor measurements of bismuth telluride nanowires grown by pulsed electrodeposition. Phys. Status Solidi - Rapid Res. Lett. 2010; (4): 43–45.
26. Jagadale AD, Kumbhar VS, Bulakhe RN, Lokhande CD. Influence of electrodeposition modes on the supercapacitive performance of Co3O4electrodes. Energy, 2014; (64): 234–241.
27. Fleurial JP, Borshchevsky A, Ryan MA, Phillips WM, Snyder JG, Caillat T, Kolawa A, Herman JA, Mueller P, Nicolet M. Development of thick-film thermoelectric microcoolers using electrochemical deposition. Thermoelectr. Mater, 1998; 493-445.
28. Walsh FC, Herron ME. Electrocrystallization and electrochemical control of crystal growth : fundamental considerations and electrodeposition of metals. J. Phys. D Appl. Phys, 1991; (24): 217–225.
29. Prieto AL, Sander MS, Martín-González MS, Gronsky R, Sands T, Stacy AM. Electrodeposition of Ordered Bi_2 Te_3 Nanowire Arrays. J. Am. Chem. Soc, 2001; (123): 7160–7161.
30. Martín-González MS, Prieto AL, Gronsky R, Sands T, Stacy AM. Insights into the Electrodeposition of Bi2Te 3. J. Electrochem. Soc, 2002; (149): C546.
31. Hodes G. Chemical solution deposition of semiconductor films. Marcel Dekker, 2003.
32. Chopra KL. Thin Film Phenomena McGraw Hill Book Company, New York, 1969; 270
33. Cao X, Gu L, Zhuge L, Qian W, Zhao C, Lan X, Sheng W, Yao D. Template-free preparation and characterization of hollow indium sulfide nanospheres. Colloids Surfaces A Physicochem. Eng. Asp, 2007; (297): 183–190.
34. Takahashi M, Kojima M, Sato S, Ohnisi N, Nishiwaki A, Wakita K, Miyuki T, Ikeda S, Muramatsu Y. Electric and thermoelectric properties of electrodeposited bismuth telluride (Bi2Te3) films. J. Appl. Phys, 2004; (96): 5582–5587.